

LookWhere? Efficient Visual Recognition by Learning Where to Look and What to See from Self-Supervision

• Anthony Fuller¹ • Yousef Yassin¹

Junfeng Wen¹ Daniel G. Kyrollos¹ Tarek Ibrahim¹

★ James R. Green¹ ★ Evan Shelhamer^{1,2,3}

Carleton University¹ University of British Columbia² Vector Institute³

• Co-first author ★ Co-advising author

Abstract

Vision transformers are ever larger, more accurate, and more expensive to compute. The expense is even more extreme at high resolution as the number of tokens grows quadratically with the image size. We turn to adaptive computation to cope with this cost by learning to predict *where* to compute. Our LookWhere method divides the computation between a low-resolution selector and a high-resolution extractor *without ever processing the full high-resolution input*. We jointly pretrain the selector and extractor *without task supervision* by distillation from a self-supervised teacher, in effect, learning where and what to compute simultaneously. Unlike prior token reduction methods, which pay to save by pruning already-computed tokens, and prior token selection methods, which require complex and expensive per-task optimization, LookWhere economically and accurately selects and extracts transferrable representations of images. We show that LookWhere excels at sparse recognition on high-resolution inputs (Traffic Signs), maintaining accuracy while reducing FLOPs by up to $34\times$ and time by $6\times$. It also excels at standard recognition tasks that are global (ImageNet classification) or local (ADE20K segmentation), improving accuracy while reducing time by $1.36\times$. Code and weights: <https://github.com/antofuller/lookwhere>

1 Introduction: A Look through Self-Supervised Eyes

Self-supervised computer vision models can identify informative inputs, as shown in Fig. 1, by **what** DINOv2 [1] attends to and **where**; all without any knowledge of the task to be done. In short, these methods solve their own learning problems: given one view of visual data, predict another (by reconstructive [2, 3, 4, 5, 6] or contrastive learning [1, 7, 8, 9]). When learned at scale, they attend to the visually interesting by identifying what is informative for their predictions; importantly, this input may be sparser than the full input, especially at high resolution, offering an opportunity for efficiency.

In this work, we reduce the computation for recognition by *predicting* this visual interest without *fully processing* the input. We rely on attention and representation in the eyes of the self-supervised model to learn both where to look, with an efficient **selector** of locations, and what to see, with an expressive **extractor** of representations. To do so, we propose **LookWhere**: a framework for self-supervised adaptive computation that factorizes where and what, for learning and inference, with paired selector-extractor models. Our selector and extractor together represent a high-res input given ❶ a **low-res** version and ❷ a sparse set of **high-res** patches selected from the high-res version. Our novel selector-extractor architecture and what-where distillation training effectively approximate deep self-supervised representations with efficient adaptive predictions.

LookWhere applies to imagery of any size, but can help most at high resolution. High resolution (with pixel dimensions of >1000 on a side) is now common in photography [10], remote sensing

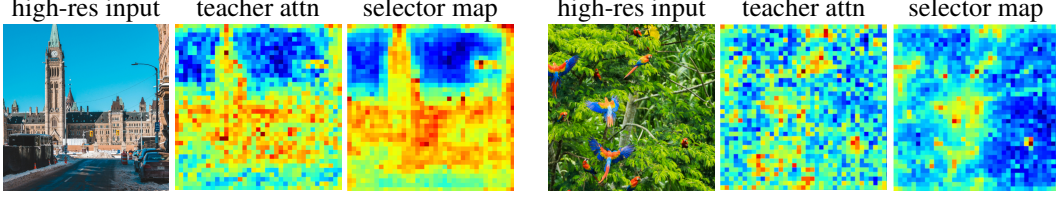


Figure 1: **Attention as Supervision.** Self-supervised models (like DINOv2 [1]) learn *what* is visually interesting without tasks or labels. We use a last step of their deep computation, the final attention map, to start ours; supervising an efficient selector that predicts *where* to process for adaptive computation.

[11], autonomous driving [12, 13], medical imaging [14, 15], and more. These high-resolution inputs offer *detail* and *context* to improve recognition [16, 17, 18, 19], but high-res computation is costly.

This cost has led to active research on adaptive computation for efficiency. These works, and ours, are motivated by the intense computation of vision transformers/ViTs [20, 21], and the opportunity in their structure: by first converting an image into tokens, then only applying pair-wise attention and token-wise FFN operations, the amount of computation scales directly with the number of tokens (quadratically for pair-wise and linearly for token-wise). Each token eliminated is efficiency gained.

LookWhere improves on existing methods for token reduction [22, 23, 24, 25, 26], and token selection [27, 28, 29, 30] in its efficiency and simplicity. Unlike token reduction methods, it never processes all input tokens, which saves computation (especially on high-res inputs). Unlike prior token selection methods, it is efficient and straightforward to pretrain and finetune. Unlike both, it jointly pretrains its selector-extractor models for transfer across diverse visual recognition tasks.

We show that LookWhere delivers state-of-the-art (SoTA) accuracy/efficiency trade-offs in comparisons and controlled experiments across tasks and resolutions. We measure its efficiency during testing and training, and find it achieves these results with the least per-task training computation. We first demonstrate LookWhere in standard benchmarks (ImageNet [31], ADE20K [32]) to prove its effectiveness. Then, we demonstrate LookWhere for high-resolution data on an established special-purpose benchmark (Traffic Signs [33]) to emphasize when adaptive computation is needed.

2 Method: Selector-Extractor Computation and What-Where Distillation

LookWhere accelerates inference by approximating full, deep representations with adaptive computation of predictions learned from distillation. The selector predicts where to look, the extractor predicts what to see, and each learns by distillation from the attention and tokens of a self-supervised teacher (Fig. 2). We call this novel joint learning scheme **what-where** distillation.

The selector and extractor work in tandem to efficiently extract task-specific representations, given minimal finetuning, based on their self-supervised pretraining of what and where to compute. We first explain inference with the selector and extractor models and their computation (Sec. 2.1). Next, we explain finetuning for a task (Sec. 2.2). Last, we explain pretraining (Sec. 2.3), which is needed just once for a visual domain to enable fast task-wise finetuning and deployment.

We review ViT computation and notation as a prerequisite for our adaptive computation of ViTs. This brief summary clarifies the computations that LookWhere approximates and accelerates.

Patchification. To process an image of dimensions $R \times R$ with C channels, ViTs split the image into an $N \times N$ grid of patches $\mathbb{R}^{R \times R \times C} \rightarrow \mathbb{R}^{N \times N \times P \times P \times C}$ where P is the resolution of a patch. This grid is then flattened into a sequence of N^2 patches, each of which is linearly projected to a D -dimensional embedding called a *token* $\mathbb{R}^{N \times N \times P \times P \times C} \rightarrow \mathbb{R}^{N^2 \times D}$. The patch tokens $x_{pat} \in \mathbb{R}^{N^2 \times D}$ are now ready for attention and feedforward network (FFN) computation.

Computation. ViTs process the tokens like a generic transformer: through a stack of architecturally-identical layers composed of pair-wise self-attention and token-wise FFN operations. The computational cost scales with tokens: self-attention scales quadratically and the FFN scales linearly.

Attention. Self-attention applies three learned linear projections to each token in the sequence, producing query, key, and value vectors. The dot product similarity between queries, and keys is the “attention” for the pair. The output for each query is the weighted sum of the values given by the

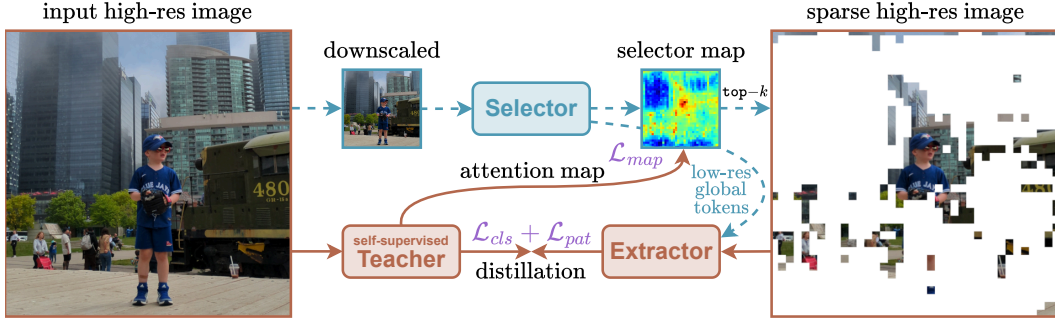


Figure 2: **LookWhere is trained by distillation** from a self-supervised teacher to learn *where* to compute, from the attention map, and *what* to compute, from the class and patch token representations. Only the teacher sees the high-res input to make its attention and tokens for the losses. The selector predicts *where* to look from the low-res input. The extractor predicts *what* to see (e.g. a boy in a hat and jersey, a coffee cup, ...) from the top k high-res patches (and low-res tokens) from the selector.

normalized attention for all pairs. (This is normally repeated across H distinct “heads”.) Tokens with *lower* attention add *less* to these sums, and raise the potential for efficiency by not computing them.

Global Tokens. Special tokens summarize *global* information to complement the local information in the patch tokens. ViTs augment the patch sequence $x_{pat} \in \mathbb{R}^{N^2 \times D}$ with a learnable “class” token $x_{cls} \in \mathbb{R}^D$, and this technique can extend to multiple “register” tokens $x_{reg} \in \mathbb{R}^{G \times D}$ for G tokens [34].

The full token sequence is $x \triangleq (x_{cls}, x_{reg}, x_{pat}) \in \mathbb{R}^{(1+G+N^2) \times D}$, and its length is dominated by the N^2 patch tokens. This is the opportunity for adaptive computation: fewer tokens, less computation.

2.1 Selector-Extractor Inference with Split Resolution Computation

LookWhere factorizes inference into a low-resolution *selector* for *where* to compute and a high-resolution *extractor* for *what* to compute. The selector operates on a low-resolution edition of the input to predict the locations of informative patches—producing a *selector map*—and also generates low-resolution summaries of the input. Only the top k most informative patches are selected from the high-resolution input. The extractor processes only these selected patches and re-uses the provided low-resolution summaries to predict a complete representation of the high-resolution input without ever processing all its pixels.

LookWhere admits a variety of architectures for the selector and extractor. Both must be differentiable for end-to-end learning. The selector should be fast in order to efficiently choose and provide the input for the extractor. The extractor should be able to harness spatial sparsity to accelerate its computation of the selected input. We satisfy these considerations by choosing ViTs for both.

The selector’s input and depth are reduced for efficient computation. We resize the input to a smaller R_{low} , and truncate the model to its first L_{low} layers; both modifications compound for higher efficiency. The selector produces latents $z_{low} \in \mathbb{R}^{(1+G+N_{low}^2) \times D}$, where the N_{low}^2 patch tokens are mapped by FFN to N_{high}^2 patch importance scores $\mathbb{R}^{N_{low}^2 \times D} \rightarrow \mathbb{R}^{N_{high} \times N_{high}}$ to yield the selector map \hat{A}_{high} .

For effective extractor computation, we take high-resolution and low-resolution inputs and maintain higher capacity. The top k locations in \hat{A}_{high} are selected as patches in the high-resolution input. The extractor tokenizes only the selected patches into $x_{high}^{pat} \in \mathbb{R}^{k \times D}$ and re-uses the selector’s low-resolution global tokens z_{low}^{cls} and z_{low}^{reg} (to replace the extractor’s own x_{cls} and x_{reg} without more computation). Given these high-resolution and low-resolution tokens, the extractor computes its patch token and global token representations following standard ViT inference. We choose the ViT-B architecture for sufficient capacity to represent what is in the input. The extractor outputs latents $\hat{z}_{high} \in \mathbb{R}^{(1+G+k) \times D}$. For a full representation of the high-resolution input, the sparse set of patch tokens are then spatially interpolated to the high-resolution grid $\hat{z}_{high} \in \mathbb{R}^{(1+G+N_{high}^2) \times D}$.

Task-specific modeling finally outputs predictions \hat{y} from \hat{z}_{high} depending on the details of the task.

2.2 Finetuning LookWhere for a Task by Supervised Learning

To apply LookWhere to a given task, we (1) add a task-specific predictor to the extractor and (2) finetune the extractor-predictor by supervised learning. For simplicity, a linear model on the extractor representation suffices to map from its global class token or local patch tokens to the output space. Finetuning LookWhere is highly efficient: we only update the predictor-extractor without updating the selector or needing the teacher. Having already pretrained our selector-extractor to approximate the self-supervised teacher, we can finetune only what they compute (the representation) for the task while sharing where they compute (the adaptive computation) across tasks. The selector further accelerates finetuning: its adaptive computation continues to reduce high-resolution processing at every step. LookWhere is more efficient during inference and during finetuning.

2.3 Pretraining by What-Where Distillation of Self-Supervision

Distillation trains a student model to predict a reference output from a teacher model [35]. LookWhere trains its selector and extractor as a pair of students to approximate a deep self-supervised model as the teacher. We distill a self-supervised model for accuracy, efficiency, and transferability. Self-supervised visual representations are now effective for many tasks [1, 5, 7, 36, 37, 38, 39]. Furthermore, their attention maps can identify informative patches in images (per our Fig. 1 and prior analyses [1, 34]). While their computation is expensive, our learned approximation need not be due to adaptive computation and the architectural decoupling of the selector-extractor enabled by distillation.

We propose simultaneous distillation of where and what to compute. We distill where from the teacher attention and what from the teacher representation. The teacher fully processes the high-resolution input to provide the attention and representation for learning. By distilling the teacher’s attention, the selector learns to predict the location of deep, salient information given only shallow, low-resolution input. The extractor learns to predict the full representation of the high-resolution input, given only sparse high-resolution tokens and the selector’s low-resolution global tokens, by distilling the teacher representation. We pretrain the selector and extractor jointly and in parallel from partial inputs that are more efficient to compute. Note that the selector and extractor learn to predict the representation of an image they never fully see, which is itself a self-supervised task: the masked reconstruction of the representation from only partial inputs and computations. These partial inputs and computations make pretraining more efficient because only the teacher representation is extracted at high resolution.

Teacher. We choose DINOv2 [1] as the teacher for its ViT architecture and internet-scale pretraining on diverse images without annotations. We use the variant with $G=4$ register tokens to reduce attention artifacts [34], as we use its attention to train the selector. The teacher processes inputs at resolution $R_{\text{high}}=518$ with patch size $P=14$ for a grid of $N_{\text{high}}=37$ patches. (This is unaltered from DINOv2.) To distill its attention, we extract the unnormalized attention among its patch tokens at the last layer and then average over queries and heads. This approximates where patch tokens contributed to the deepest teacher representation. To distill its representation, we extract the class and patch tokens at the last layer: $z_{\text{high}} \in \mathbb{R}^{(1+N_{\text{high}}^2) \times D}$. We never update the teacher: its parameters are fixed.

Losses and Updates. We train LookWhere jointly with three losses for what to compute, by distillation of the class token and patch tokens, and where to compute, by distillation of attention.

- *Class Token Distillation:* We distill the teacher’s class token via mean-squared error (MSE): $\mathcal{L}_{cls} = \text{MSE}(z_{\text{high}}^{cls}, z_{\text{high}}^{cls})$. This trains the selector and extractor to learn global representations of the high-res input, given the low-res input and selected high-res patches.
- *Patch Token Distillation:* We distill the teacher’s patch representations via the mean-squared error (MSE): $\mathcal{L}_{pat} = \text{MSE}(z_{\text{high}}^{pat}, z_{\text{high}}^{pat})$. This trains the selector and extractor to learn local representations of the high-res input, given the low-res input and selected high-res patches.
- *Attention Distillation:* We distill the teacher’s attention map via the Kullback–Leibler (KL) divergence: $\mathcal{L}_{map} = \text{KL}(\hat{A}_{\text{high}}, A_{\text{high}})$. This trains the selector to predict where the teacher computes.

Our pretraining loss is their sum $\mathcal{L} = \lambda_{cls}\mathcal{L}_{cls} + \lambda_{pat}\mathcal{L}_{pat} + \lambda_{map}\mathcal{L}_{map}$. We set $\lambda_{cls}, \lambda_{pat} = 1$, and $\lambda_{map} = 0.1$. All losses are optimized end-to-end by the extractor and selector. We update the selector and extractor jointly and in parallel without custom batching, balancing, or tuning.

Initialization. We set the selector and extractor parameters to those of the teacher: DINOv2.

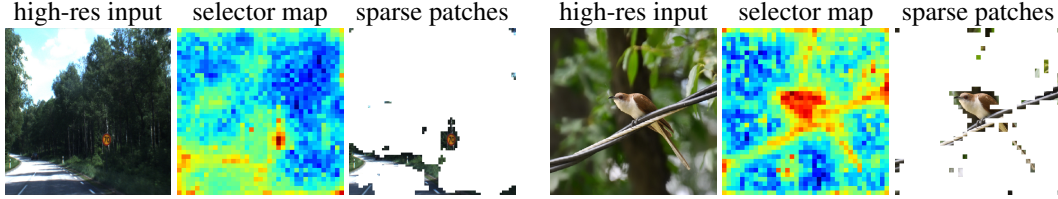


Figure 3: **Looking at Adaptive Computation.** We visualize the selector’s prediction of *where* to compute and the extractor’s sparse input for *what* to see. Left: Spatially-sparse traffic sign recognition. Right: Fine-grained bird recognition. The same selector generalizes across these images and tasks.

Table 1: **ImageNet Classification.** LookWhere is more accurate and significantly faster than SoTA adaptive computation methods for ViTs. Inference memory is equal for all models. Each cell reports the results for ViT-S/ViT-B: – = not reported and L = layer.

Method	Top-1 Acc. % \uparrow	FLOPs G \downarrow	Speed K im/s \uparrow	Avg Tok per L \downarrow
DINOv2 [1]	81.9/84.2	6.2/23.6	6.8/2.2	256
PiToMe [23] ($r=0.925$)	79.8/ -	3.1/ -	6.6/ -	128
DTEM [25] ($r=16$)	79.4/80.7	2.4/9.2	7.0/3.8	94
ATC [24] ($r=0.9$)	79.9/82.0	4.0/15.3	0.4/0.4	169
LTRP [30] ($\text{keep}=0.75$)	- /82.8	- /18.3	- /2.3	147
LookWhere ($k=128$)	80.3/83.0	3.8/14.8	9.5/3.2	128

Table 2: **ADE20K Segmentation.** We compare three levels of adaptive computation (r , k): LookWhere is more accurate & efficient at each level.

Method	mIoU % \uparrow	FLOPs G \downarrow	Speed K im/s \uparrow
DINOv2 [1]	46.8	46.7	0.9
DTEM [25] ($r=0.5$)	38.9	19.0	0.7
LookWhere ($k=512$)	40.6	14.6	2.0
DTEM [25] ($r=0.4$)	42.6	22.3	0.6
LookWhere ($k=768$)	43.3	23.1	1.4
DTEM [25] ($r=0.3$)	44.3	25.8	0.5
LookWhere ($k=1024$)	44.6	32.8	1.0

3 Experiments: Accuracy & Efficiency

We evaluate on standard visual recognition benchmarks in Sec. 3.1, to confirm that LookWhere is generally accurate and efficient, and on high-resolution benchmarks in Sec. 3.2, to measure adaptive computation when efficiency is key. The standard benchmarks, ImageNet-1K classification [31] and ADE20K semantic segmentation [32], are ubiquitous in deep learning for vision. The high-resolution benchmarks, Swedish Traffic Signs [33] and the Caltech-UCSD Birds [40], evaluate spatially-sparse classification tasks as established by existing work on adaptive computation. We then analyze our choice of self-supervision and ablate our selector, extractor, and distillation in Sec. 3.4.

Fig. 3 shows our selector’s choice of high-resolution patches (see Appendix A.4 for more examples). Recall that we only update our extractor for each task, and rely on the selector to generalize when predicting where to compute.

Comparisons and Baselines. We choose state-of-the-art comparisons encompassing both token *reduction* (PiToMe [23], ATC [24], and DTEM [25]) and token *selection* (DPS [28], and IPS [29]). We review their sophisticated adaptive computation methods in Sec. 4, and Appendix A.1.

Measuring Computation. We measure throughput speed, FLOPs, and peak memory usage for a complete accounting of computational efficiency. We profile computation with the official `torch.profiler` tool, the reference implementations of all methods, and an RTX 4090 GPU.

3.1 Comparison Experiments on Standard Recognition Benchmarks

We apply our standard finetuning of LookWhere (Sec. 2.2) to update the extractor for image classification on ImageNet-1K [41] and semantic segmentation on ADE20K [32]. We include DINOv2 as a non-adaptive baseline and as the teacher for LookWhere during pretraining.

ImageNet Classification. This standard benchmark of accuracy and efficiency is also used for adaptive computation with ViTs (Tab. 1). We follow prior work [42, 25, 23, 43] and finetune for 30 epochs at 224^2 px resolution. LookWhere achieves the best accuracy and speed for adaptive computation at ViT-S and ViT-B scales with comparable memory and FLOPs. For top speed with the smaller ViT-S model, it delivers $1.36\times$ faster computation than the second fastest method (DTEM).

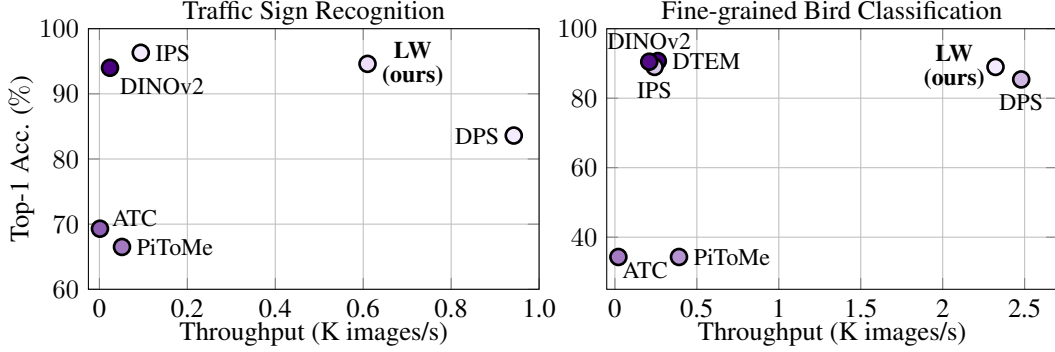


Figure 4: **High-Resolution Recognition on Traffic Signs and Birds (CUB).** We plot the accuracy and throughput of LookWhere, its teacher (DINOv2), and state-of-the-art token reduction and selection methods. LookWhere reaches the Pareto frontier for sparse object recognition (left) and for fine-grained classification (right). To more fully measure computation, we color each point by memory usage (darker is higher/less efficient). Please see Appendix A.2 for more details and results.

ADE20K Segmentation. This standard benchmark of semantic segmentation / pixel classification (Tab. 2) requires more spatial precision than image classification. Most adaptive computation methods do not tackle this more challenging task, but DTEM [25] does, so we compare in their setting. We vary the amount of computation to measure the accuracy/efficiency trade-off. LookWhere has better accuracy at $\geq 2\times$ higher speed compared to DTEM.

For both tasks, adaptive computation improves efficiency, but with a trade-off. Without adaptive computation, DINOv2 is the most accurate but less efficient. With adaptive computation, LookWhere achieves the best accuracy and highest efficiency.

3.2 High-Resolution Benchmarks with Spatial Sparsity: Where Efficiency is Key

We evaluate the accuracy, efficiency, and generalization of LookWhere on high-resolution inputs. Specifically we choose datasets with spatial sparsity or fine-grained detail, and finetune while limiting the ratio of high-resolution tokens computed. For these experiments we set the number of patches k for LookWhere to process only 10% of the high-resolution input. This sparsity at high-resolution tests our selector’s ability to prioritize and improve efficiency by adaptive computation.

In these experiments, we control for factors like backbone architecture (DINOv2), training time (30 epochs of finetuning), and input size (square crops following DINOv2 pretraining). We standardize in this way for clarity of comparison; please see the end of this section for more details.

Spatially-Sparse Recognition of Traffic Signs. The Traffic Signs dataset [33] has large images of signs and class labels. The variable and often small size of the signs results in spatial sparsity. We follow the established adaptive computation benchmark [28, 29, 44] of recognizing speed limit signs as 50, 70, or 80 km/h or no sign. We set the input size to be square: 994×994 px.

LookWhere strikes the best accuracy-speed balance across all methods (Fig. 4, left). LookWhere is competitive with the state-of-the-art: it rivals IPS in accuracy while reducing inference time by $6\times$ and FLOPs by $34\times$, although IPS reaches 1.1% higher accuracy with more computation. LookWhere exceeds its teacher DINOv2 in efficiency *and* accuracy, even though the teacher processes the full input. Note that longer training and additional tuning can achieve higher accuracy for all methods (including LookWhere, DPS, and IPS) but departs from this controlled setting for fair comparisons.

Fine-Grained Recognition of Birds. We evaluate how well LookWhere represents visual detail by experimenting with fine-grained recognition on the Caltech-UCSD Birds (CUB-200-2011) dataset [40] of 200 bird species in 11,788 images. This common benchmark has been adopted for adaptive computation [28, 45]. We set the input size to square 518×518 px following the default for DINOv2.

LookWhere reaches the top accuracy, least FLOPs, and fastest speed among adaptive computation methods (Fig. 4, right). Relative to its DINOv2 teacher, which processes all patches, LookWhere has nearly equal accuracy at $\frac{1}{10}$ of the patches for more efficiency in speed, memory, and FLOPs.

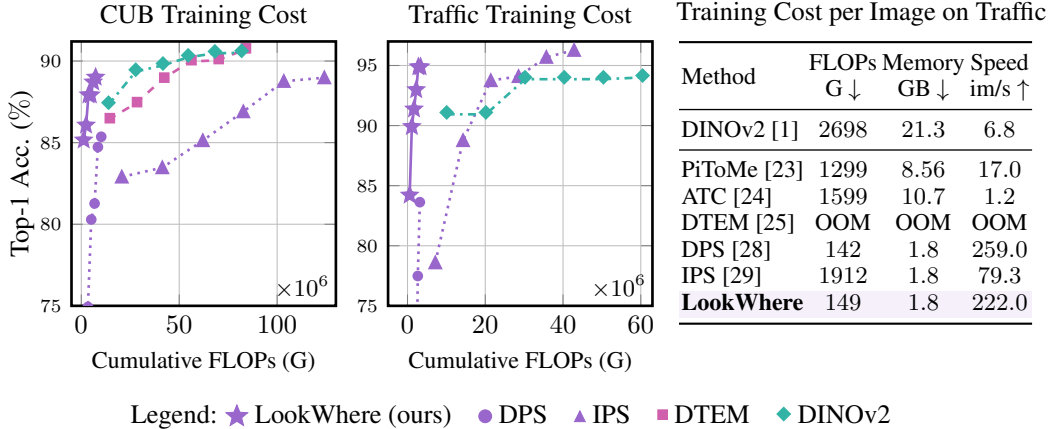


Figure 5: **Finetuning Computation.** We plot (left) the accuracy and cumulative FLOPs for training adaptive computation methods on high-res data, and report (right) the cost per image. LookWhere rivals or bests the accuracy of SoTA token reduction and selection methods at a fraction of the cost.

Experiment Setup for Controlled Comparisons. We finetune all models for 30 epochs with the AdamW optimizer [46]. All methods use the DINOv2 (ViT-Base) backbone, which is the same as the teacher for LookWhere. We tune all methods equally. For each method, we sweep learning rates $\{2e-5, 5e-5, 8e-5, 1e-4\}$, selecting the best result based on final test accuracy. See Appendix A.2 for hyperparameter settings (e.g., token reduction/selection amounts) and exhaustive results.

3.3 Pretraining

We pretrain on ImageNet-1K [41]. We train ViT-Base for 200 epochs and ViT-Small for 400 epochs. We augment the data with standard RandAugment [47] transformations. We evaluate the teacher on every input for its attention and representation. We set the selector’s input size $R_{\text{low}}=154$ and depth $L_{\text{low}}=3$ for efficiency; these perform well, and LookWhere works with different choices. At each step, we sample $k \in [16, 128]$ (out of $N_{\text{high}}^2=1,369$ tokens per image) for transferrable adaptive computation at high resolution. We optimize by AdamW [46] with the same learning rate for the selector and extractor. Please see Appendix A.2 for full details.

Our what-where distillation is generally robust to pretraining settings. It works well across learning rates, loss weights, selector sizes, and the choice of low-res tokens to share in the selector and extractor.

3.4 Analysis and Ablations

Accounting for Computation. Efficiency depends on input size and hardware acceleration. For time, LookWhere is faster at low-res (e.g., 224^2 px) and higher-res (e.g., $>512^2$ px). For FLOPs, LookWhere is often equal or better, but at low-res its selector is relatively costly, and the total can exceed the FLOPs of methods without such a predictor. For memory, LookWhere is equal or better at low-res and high-res, and can reduce training memory by $>5\times$. While these metrics usefully summarize computation, on close examination, the type and hardware compatibility of operations impact efficiency. LookWhere relies only on the accelerated GPU computation of standard ViT layers. However, PiToMe, DTEM, and ATC all rely on clustering algorithms, which are FLOP efficient yet slower on current hardware. As a result, at high-res LookWhere is more time/FLOP/memory efficient than these SoTA methods with $>10\times$ the speed and $>5\times$ reduction in FLOPs and memory (Fig. 5).

3.4.1 Where to Look for Supervision of Where to Look?

Our selector drives adaptive computation by predicting where to process high-res patches. How the selector learns is fundamental to our method, so we investigate the choice of supervision for it.

Attention Maps as Oracle Selectors. ViTs compute *thousands* of 2D attention maps over patch tokens. We test 35 salient choices of teacher attention maps and their aggregations as substitutes

for the selector. Specifically, we pretrain LookWhere ViT-S extractors by selecting high-res patches using teacher attention maps instead of selector predictions. These experiments train on ImageNet for 100 epochs. To check generality across tasks, we evaluate via k NN for classification over class token representations on ImageNet-HR [48] (a high-res ImageNet-1K test set) and k NN for segmentation over patch token representations on ADE20K.

Results across Layers and Queries. Fig. 6 shows how accuracy depends on which layers and query tokens to choose for the attention maps. For layers, accuracy generally improves with depth. For query tokens, classification is insensitive ($< \pm 1\%$), but segmentation is more sensitive ($> \pm 3\%$). We choose the teacher’s last layer attention over patch tokens: it balances the accuracy of both tasks.

Classification		Layer Aggregation				
Query Aggregation		first half	last half	last third	last only	all layers
	cls	69.3	72.1	72.4	73.4	71.9
	reg	69.1	70.2	71.3	73.4	69.6
	pat	67.0	71.9	72.0	73.1	71.6
	cls+reg	69.3	70.4	72.7	73.7	71.2
	cls+pat	69.6	72.6	73.0	73.7	72.0
	reg+pat	68.9	71.3	72.1	74.3	70.9
	cls+reg+pat	69.2	72.2	73.0	73.4	71.6

Segmentation		Layer Aggregation				
Query Aggregation		first half	last half	last third	last only	all layers
	cls	64.3	63.8	63.4	63.4	64.5
	reg	64.5	64.9	65.0	64.1	65.2
	pat	65.5	67.4	67.3	66.2	67.5
	cls+reg	64.5	64.7	64.8	63.2	65.2
	cls+pat	65.4	65.7	64.9	63.7	65.7
	reg+pat	65.1	66.0	66.1	64.6	66.1
	cls+reg+pat	64.9	65.8	65.2	63.8	65.8

Figure 6: **Teacher Attention for Selection.** We evaluate teacher attention maps as selector maps to choose distillation targets. For classification (k NN on ImageNet-HR), the deepest attention maps and class queries perform best. For segmentation (k NN on ADE20K), averaging over all layers and patch queries perform best. We choose the last layer’s patch token attention maps to balance the tasks.

3.4.2 Ablating Selector-Extractor Architecture and What-Where Distillation

(a) Deeper selectors & larger inputs are more accurate but slower.

depth	res.	cls.	seg.
1	252 ²	66.2	60.5
3	252 ²	69.7	64.7
3	154 ²	68.8	62.7
6	154 ²	69.7	63.0
6	98 ²	63.0	60.2
12	98 ²	69.6	61.0
12	42 ²	47.3	54.6

(b) Training the selector map on teacher attention *alone* is best.

case	cls.	seg.
none (stop grad)	63.0	60.2
Gumbel Top-K [49]	61.4	58.9
REINFORCE [50]	61.8	59.6

(c) Giving the extractor global tokens from the selector helps.

case	cls.	seg.
none	60.7	56.9
cls-only	62.2	58.7
reg-only	62.0	59.8
cls+reg	63.0	60.2

(d) Random selection hurts. Varying k during finetuning enables flexible inference at different k .

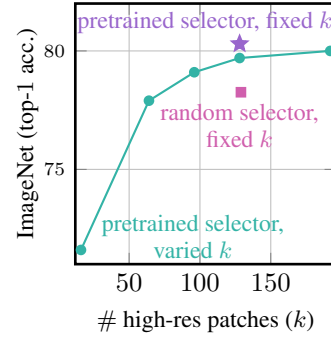


Figure 7: **Ablating Architecture and Training** “cls.” = k NN image/class token classification on ImageNet-HR (top-1 acc.) and “seg.” = k NN local/patch token classification on ADE20K (top-1 acc.). Default settings are shared across ablations; final setting is used on downstream experiments. Subfigure (d) finetunes on ImageNet and evaluates on ImageNet-Val for comparability with Tab. 1.

Design Choices. We ablate four design choices of our architecture and pretraining (Fig. 7). We experiment with 518² resolution, ViT-S architecture, and $k=72$ (out of 1,369 high-res patches). (1) We vary the depth and input size of the selector (a). Larger inputs tend to help more than deeper architecture, so we choose 154² px resolution a 3 layers. (2) We experiment with training the selector map end-to-end from the extractor’s distillation losses alongside the attention distillation loss. We try REINFORCE [50] (inspired by PatchDrop [27]), and Gumbel Top- k [49] for this purpose and observe no improvement from either (b). (3) We confirm the effectiveness of passing global tokens from the selector to the extractor for efficiency (c). (4) We measure the trade-off in class token vs. patch token loss weights across classification and segmentation (see Appendix A.3).

Random Selection Ablation. We ablate our selector by selecting high-res patches at random. On Traffic Signs, accuracy **drops by 25%**, which is only marginally better than choosing the majority

class. The drop on CUB is 11%, and on ImageNet, it is 2.1% (Fig. 7(d)). The smaller drop on ImageNet could be due to its object-centric images making *where* less important.

Varying k for Flexibility. We randomly vary k by sampling from $[1, 256]$ during finetuning on ImageNet. This enables choosing k at inference for faster/more accurate computation (Fig. 7(d)).

4 Related Work

Token reduction drops or merges already-computed tokens layer-by-layer to save *further* computation. Many of these methods cleverly combine similar tokens by soft bipartite matching algorithms [22, 23, 26, 51, 25], while others incorporate dynamic filtering [52, 53] or differentiable pruning [43]. Nonetheless, such *gradual* reduction requires processing all tokens at the first layer, nearly all at the second, and so on. This is already too much in our case: *any* processing of *all* tokens is too expensive at high resolution. By contrast, our selector processes a low-resolution input, and then our extractor receives a small set of high-resolution patches. LookWhere never processes the full-resolution input to attain efficiency unobtainable by reduction.

Token selection chooses the inputs for computation, and so can save more, but must learn how to select and do so efficiently. Prior works scale to megapixel images but require complex and expensive per-task optimization [27, 28, 29]. IPS [29] iterates over sets of patches to identify the most salient, which reduces memory but still takes time. DPS [28] and PatchDrop [27] train predictors that process low-resolution versions of the input to score high-resolution patches by discrete optimization. While efficient for inference, their optimization requires sampling, careful tuning of gradient approximation [50, 54], and multi-stage training (PatchDrop). LookWhere also processes low and high resolutions for efficient inference, but with simple and efficient training during both pretraining (by distillation) and finetuning (by extractor-only updates).

Self-supervision for Adaptive Computation. Most existing token reduction and selection methods rely on task-specific optimization that does not harness transfer across tasks. LTRP [30] instead pretrains a general selector by self-supervision, like LookWhere, but lacks a general extractor and scores patches differently. Specifically, LTRP relies on multiple forward passes over perturbed inputs to measure the patch-wise sensitivity of a self-supervised model (MAE [2]) to supervise its selector. This results in expensive pretraining ($>10\times$ ours) without an extractor to transfer. By contrast, LookWhere directly distills the teacher’s attention and representation, which only needs *one* forward pass to compute. Furthermore, LookWhere simultaneously pretrains the selector and extractor for efficient re-use and transfer across tasks.

Distillation. Many works train the attention maps of students to mimic the attention maps of teachers [55, 56, 57, 58], and last layer teacher attention maps in particular [59]. However, our what-where distillation trains our student, the selector, to predict a single map that summarizes multiple teacher attention maps. This strategy allows our selector to predict a map at higher resolution than its input—e.g., receiving $N_{\text{low}} \times N_{\text{low}}$ patches and predicting an $N_{\text{high}} \times N_{\text{high}}$ map. Furthermore, existing methods do not distill attention for adaptive computation: we are the first to turn self-supervised attention maps into the supervision of how to prioritize tokens for adaptive computation.

5 Conclusion

We introduce our selector-extractor architecture and what-where distillation for accurate, efficient, and general adaptive computation on diverse visual recognition tasks. LookWhere is simple but effective: a selector predicts a 2D map (*where* to look) for an extractor that predicts full-res image representations (*what* to see). This simplicity enables efficiency on current hardware: LookWhere applies standard transformer operations used just right. Together, our selector & extractor represent images they never fully see for efficient finetuning and deployment, especially at high resolutions.

Limitations and Future Work. There is more to learn for selection and there are more dimensions for adaptive computation. LookWhere does not finetune the selector. Although this achieves SoTA results, by pretraining a task-general selector, finetuning a task-specific selector could do better. Our selector-extractor is only spatial, but could be temporal (LookWhen) for video or spectral (LookWhich) for remote sensing bands.

Acknowledgements

AF is primarily supported by an NSERC PGS-D scholarship. ES is supported by a Canada CIFAR AI Chair. YY is primarily supported by an Ontario Graduate Scholarship (OGS) and a Vector Scholarship in AI. Resources used in preparing this research were provided, in part, by the Province of Ontario, the Government of Canada through CIFAR, and companies sponsoring the Vector Institute. We thank the Google TPU Research Cloud (TRC) for providing the TPUs on which we conducted all pretraining experiments. We thank Eric Tzeng for their helpful review and feedback on the experiments and analysis.

References

- [1] Maxime Oquab, Timothée Darcet, Théo Moutakanni, Huy Vo, Marc Szafraniec, Vasil Khalidov, Pierre Fernandez, Daniel Haziza, Francisco Massa, Alaaeldin El-Nouby, et al. Dinov2: Learning robust visual features without supervision. *arXiv preprint arXiv:2304.07193*, 2023.
- [2] Kaiming He, Xinlei Chen, Saining Xie, Yanghao Li, Piotr Dollár, and Ross Girshick. Masked autoencoders are scalable vision learners. In *Proceedings of the IEEE/CVF conference on computer vision and pattern recognition*, pages 16000–16009, 2022.
- [3] Hangbo Bao, Li Dong, Songhao Piao, and Furu Wei. Beit: Bert pre-training of image transformers. *arXiv preprint arXiv:2106.08254*, 2021.
- [4] Zhenda Xie, Zheng Zhang, Yue Cao, Yutong Lin, Jianmin Bao, Zhuliang Yao, Qi Dai, and Han Hu. Simmim: A simple framework for masked image modeling. In *Proceedings of the IEEE/CVF conference on computer vision and pattern recognition*, pages 9653–9663, 2022.
- [5] Mahmoud Assran, Quentin Duval, Ishan Misra, Piotr Bojanowski, Pascal Vincent, Michael Rabbat, Yann LeCun, and Nicolas Ballas. Self-supervised learning from images with a joint-embedding predictive architecture. In *Proceedings of the IEEE/CVF Conference on Computer Vision and Pattern Recognition*, pages 15619–15629, 2023.
- [6] Yibing Wei, Abhinav Gupta, and Pedro Morgado. Towards latent masked image modeling for self-supervised visual representation learning. In *European Conference on Computer Vision*, pages 1–17. Springer, 2024.
- [7] Kaiming He, Haoqi Fan, Yuxin Wu, Saining Xie, and Ross Girshick. Momentum contrast for unsupervised visual representation learning. In *Proceedings of the IEEE/CVF conference on computer vision and pattern recognition*, pages 9729–9738, 2020.
- [8] Ting Chen, Simon Kornblith, Kevin Swersky, Mohammad Norouzi, and Geoffrey E Hinton. Big self-supervised models are strong semi-supervised learners. *Advances in neural information processing systems*, 33:22243–22255, 2020.
- [9] Xinlei Chen and Kaiming He. Exploring simple siamese representation learning. In *Proceedings of the IEEE/CVF conference on computer vision and pattern recognition*, pages 15750–15758, 2021.
- [10] Qianqian Shen, Yunhan Zhao, Nahyun Kwon, Jeeun Kim, Yanan Li, and Shu Kong. A high-resolution dataset for instance detection with multi-view object capture. *Advances in Neural Information Processing Systems*, 36:42064–42076, 2023.
- [11] Ritwik Gupta, Shufan Li, Tyler Zhu, Jitendra Malik, Trevor Darrell, and Karttikeya Mangalam. xt: Nested tokenization for larger context in large images. In *Forty-first International Conference on Machine Learning*, 2024.
- [12] Marius Cordts, Mohamed Omran, Sebastian Ramos, Timo Scharwächter, Markus Enzweiler, Rodrigo Benenson, Uwe Franke, Stefan Roth, and Bernt Schiele. The cityscapes dataset. In *CVPR Workshop on the Future of Datasets in Vision*, volume 2, page 1, 2015.
- [13] Hongbo Zhao, Lue Fan, Yuntao Chen, Haochen Wang, Xiaojuan Jin, Yixin Zhang, Gaofeng Meng, ZHAO-XIANG ZHANG, et al. Opensatmap: A fine-grained high-resolution satellite dataset for large-scale map construction. *Advances in Neural Information Processing Systems*, 37:59216–59235, 2024.
- [14] Wisdom Ikezogwo, Saygin Seyfioglu, Fatemeh Ghezloo, Dylan Geva, Fatwir Sheikh Mohammed, Pavan Kumar Anand, Ranjay Krishna, and Linda Shapiro. Quilt-1m: One million

- image-text pairs for histopathology. *Advances in neural information processing systems*, 36:37995–38017, 2023.
- [15] Hanwen Xu, Naoto Usuyama, Jaspreet Bagga, Sheng Zhang, Rajesh Rao, Tristan Naumann, Cliff Wong, Zelalem Gero, Javier González, Yu Gu, et al. A whole-slide foundation model for digital pathology from real-world data. *Nature*, 630(8015):181–188, 2024.
 - [16] Jingdong Wang, Ke Sun, Tianheng Cheng, Borui Jiang, Chaorui Deng, Yang Zhao, Dong Liu, Yadong Mu, Minghui Tan, Xinggang Wang, et al. Deep high-resolution representation learning for visual recognition. *IEEE transactions on pattern analysis and machine intelligence*, 43(10):3349–3364, 2020.
 - [17] Chen Jin, Ryutaro Tanno, Thomy Mertzanidou, Eleftheria Panagiotaki, and Daniel C. Alexander. Learning to downsample for segmentation of ultra-high resolution images. In *International Conference on Learning Representations*, 2022.
 - [18] Lianghai Zhu, Bencheng Liao, Qian Zhang, Xinlong Wang, Wenyu Liu, and Xinggang Wang. Vision mamba: Efficient visual representation learning with bidirectional state space model. In *Forty-first International Conference on Machine Learning*.
 - [19] Penghao Wu and Saining Xie. V?: Guided visual search as a core mechanism in multimodal llms. In *Proceedings of the IEEE/CVF Conference on Computer Vision and Pattern Recognition*, pages 13084–13094, 2024.
 - [20] Alexey Dosovitskiy, Lucas Beyer, Alexander Kolesnikov, Dirk Weissenborn, Xiaohua Zhai, Thomas Unterthiner, Mostafa Dehghani, Matthias Minderer, Georg Heigold, Sylvain Gelly, Jakob Uszkoreit, and Neil Houlsby. An image is worth 16x16 words: Transformers for image recognition at scale. In *International Conference on Learning Representations*, 2021.
 - [21] Mostafa Dehghani, Josip Djolonga, Basil Mustafa, Piotr Padlewski, Jonathan Heek, Justin Gilmer, Andreas Peter Steiner, Mathilde Caron, Robert Geirhos, Ibrahim Alabdulmohsin, et al. Scaling vision transformers to 22 billion parameters. In *International Conference on Machine Learning*, pages 7480–7512. PMLR, 2023.
 - [22] Daniel Bolya, Cheng-Yang Fu, Xiaoliang Dai, Peizhao Zhang, Christoph Feichtenhofer, and Judy Hoffman. Token merging: Your vit but faster. *arXiv preprint arXiv:2210.09461*, 2022.
 - [23] Chau Tran, Duy MH Nguyen, Manh-Duy Nguyen, TrungTin Nguyen, Ngan Le, Pengtao Xie, Daniel Sonntag, James Y Zou, Binh Nguyen, and Mathias Niepert. Accelerating transformers with spectrum-preserving token merging. *Advances in Neural Information Processing Systems*, 37:30772–30810, 2024.
 - [24] Joakim Bruslund Haurum, Sergio Escalera, Graham W Taylor, and Thomas B Moeslund. Agglomerative token clustering. In *European Conference on Computer Vision*, pages 200–218. Springer, 2024.
 - [25] Dong Hoon Lee and Seunghoon Hong. Learning to merge tokens via decoupled embedding for efficient vision transformers. In *The Thirty-eighth Annual Conference on Neural Information Processing Systems*, 2024.
 - [26] Minchul Kim, Shangqian Gao, Yen-Chang Hsu, Yilin Shen, and Hongxia Jin. Token fusion: Bridging the gap between token pruning and token merging. In *Proceedings of the IEEE/CVF Winter Conference on Applications of Computer Vision*, pages 1383–1392, 2024.
 - [27] Burak Uzkent and Stefano Ermon. Learning when and where to zoom with deep reinforcement learning. In *Proceedings of the IEEE/CVF Conference on Computer Vision and Pattern Recognition*, pages 12345–12354, 2020.
 - [28] Jean-Baptiste Cordonnier, Aravindh Mahendran, Alexey Dosovitskiy, Dirk Weissenborn, Jakob Uszkoreit, and Thomas Unterthiner. Differentiable patch selection for image recognition. In *Proceedings of the IEEE/CVF Conference on Computer Vision and Pattern Recognition*, pages 2351–2360, 2021.
 - [29] Benjamin Bergner, Christoph Lippert, and Aravindh Mahendran. Iterative patch selection for high-resolution image recognition. In *The Eleventh International Conference on Learning Representations*, 2023.
 - [30] Yang Luo, Zhineng Chen, Peng Zhou, Zuxuan Wu, Xieping Gao, and Yu-Gang Jiang. Learning to rank patches for unbiased image redundancy reduction. In *Proceedings of the IEEE/CVF Conference on Computer Vision and Pattern Recognition*, pages 22831–22840, 2024.

- [31] Jia Deng, Wei Dong, Richard Socher, Li-Jia Li, Kai Li, and Li Fei-Fei. Imagenet: A large-scale hierarchical image database. In *2009 IEEE conference on computer vision and pattern recognition*, pages 248–255. Ieee, 2009.
- [32] Bolei Zhou, Hang Zhao, Xavier Puig, Tete Xiao, Sanja Fidler, Adela Barriuso, and Antonio Torralba. Semantic understanding of scenes through the ADE20K dataset. *International Journal of Computer Vision*, 127:302–321, 2019.
- [33] Fredrik Larsson and Michael Felsberg. Using fourier descriptors and spatial models for traffic sign recognition. In *Scandinavian conference on image analysis*, pages 238–249. Springer, 2011.
- [34] Timothée Darcet, Maxime Oquab, Julien Mairal, and Piotr Bojanowski. Vision transformers need registers. In *The Twelfth International Conference on Learning Representations*, 2024.
- [35] Geoffrey Hinton, Oriol Vinyals, and Jeff Dean. Distilling the knowledge in a neural network. *arXiv preprint arXiv:1503.02531*, 2015.
- [36] Anthony Fuller, Koreen Millard, and James Green. Croma: Remote sensing representations with contrastive radar-optical masked autoencoders. *Advances in Neural Information Processing Systems*, 36:5506–5538, 2023.
- [37] Gabriel Tseng, Anthony Fuller, Marlina Reil, Henry Herzog, Patrick Beukema, Favyen Bastani, James R. Green, Evan Shelhamer, Hannah Kerner, and David Rolnick. Galileo: Learning global and local features in pretrained remote sensing models, 2025.
- [38] Aiham Taleb, Winfried Loetzsch, Noel Danz, Julius Severin, Thomas Gaertner, Benjamin Bergner, and Christoph Lippert. 3d self-supervised methods for medical imaging. *Advances in neural information processing systems*, 33:18158–18172, 2020.
- [39] Xiwen Liang, Yangxin Wu, Jianhua Han, Hang Xu, Chunjing Xu, and Xiaodan Liang. Effective adaptation in multi-task co-training for unified autonomous driving. *Advances in Neural Information Processing Systems*, 35:19645–19658, 2022.
- [40] C. Wah, S. Branson, P. Welinder, P. Perona, and S. Belongie. Caltech-ucsd birds-200-2011. Technical Report CNS-TR-2011-001, California Institute of Technology, 2011.
- [41] Olga Russakovsky, Jia Deng, Hao Su, Jonathan Krause, Sanjeev Satheesh, Sean Ma, Zhiheng Huang, Andrej Karpathy, Aditya Khosla, Michael Bernstein, et al. Imagenet large scale visual recognition challenge. *International journal of computer vision*, 115:211–252, 2015.
- [42] Lingchen Meng, Hengduo Li, Bor-Chun Chen, Shiyi Lan, Zuxuan Wu, Yu-Gang Jiang, and Ser-Nam Lim. Advait: Adaptive vision transformers for efficient image recognition. In *Proceedings of the IEEE/CVF conference on computer vision and pattern recognition*, pages 12309–12318, 2022.
- [43] Yongming Rao, Wenliang Zhao, Benlin Liu, Jiwen Lu, Jie Zhou, and Cho-Jui Hsieh. Dynamicvit: Efficient vision transformers with dynamic token sparsification. *Advances in neural information processing systems*, 34:13937–13949, 2021.
- [44] Angelos Katharopoulos and François Fleuret. Processing megapixel images with deep attention-sampling models. In *International Conference on Machine Learning*, pages 3282–3291. PMLR, 2019.
- [45] Ze Yang, Tiange Luo, Dong Wang, Zhiqiang Hu, Jun Gao, and Liwei Wang. Learning to navigate for fine-grained classification. In *Proceedings of the European conference on computer vision (ECCV)*, pages 420–435, 2018.
- [46] Ilya Loshchilov and Frank Hutter. Decoupled weight decay regularization. In *International Conference on Learning Representations*, 2019.
- [47] Ekin Dogus Cubuk, Barret Zoph, Jon Shlens, and Quoc Le. Randaugment: Practical automated data augmentation with a reduced search space. In H. Larochelle, M. Ranzato, R. Hadsell, M.F. Balcan, and H. Lin, editors, *Advances in Neural Information Processing Systems*, volume 33, pages 18613–18624. Curran Associates, Inc., 2020.
- [48] Anthony Fuller, Daniel Kyrollos, Yousef Yassin, and James Green. Lookhere: Vision transformers with directed attention generalize and extrapolate. *Advances in Neural Information Processing Systems*, 37:19683–19739, 2024.

- [49] Eric Jang, Shixiang Gu, and Ben Poole. Categorical reparameterization with gumbel-softmax. *arXiv preprint arXiv:1611.01144*, 2016.
- [50] Ronald J Williams. Simple statistical gradient-following algorithms for connectionist reinforcement learning. *Machine learning*, 8:229–256, 1992.
- [51] Sanghyeok Lee, Joonmyung Choi, and Hyunwoo J Kim. Multi-criteria token fusion with one-step-ahead attention for efficient vision transformers. In *Proceedings of the IEEE/CVF Conference on Computer Vision and Pattern Recognition*, pages 15741–15750, 2024.
- [52] Benjamin Bergner, Christoph Lippert, and Aravindh Mahendran. Token crop: Faster vits for quite a few tasks. *arXiv preprint arXiv:2412.00965*, 2024.
- [53] Hongxu Yin, Arash Vahdat, Jose M Alvarez, Arun Mallya, Jan Kautz, and Pavlo Molchanov. A-vit: Adaptive tokens for efficient vision transformer. In *Proceedings of the IEEE/CVF conference on computer vision and pattern recognition*, pages 10809–10818, 2022.
- [54] Quentin Berthet, Mathieu Blondel, Olivier Teboul, Marco Cuturi, Jean-Philippe Vert, and Francis Bach. Learning with differentiable perturbed optimizers. *Advances in neural information processing systems*, 33:9508–9519, 2020.
- [55] Yang Zhou, Xu Gao, Zichong Chen, and Hui Huang. Attention distillation: A unified approach to visual characteristics transfer. *arXiv preprint arXiv:2502.20235*, 2025.
- [56] Kai Wang, Fei Yang, and Joost van de Weijer. Attention distillation: self-supervised vision transformer students need more guidance. *arXiv preprint arXiv:2210.00944*, 2022.
- [57] Alex Li, Yuandong Tian, Beidi Chen, Deepak Pathak, and Xinlei Chen. On the surprising effectiveness of attention transfer for vision transformers. *Advances in Neural Information Processing Systems*, 37:113963–113990, 2024.
- [58] Xuan Gong, Abhishek Sharma, Srikrishna Karanam, Ziyang Wu, Terrence Chen, David Doremann, and Arun Innanje. Ensemble attention distillation for privacy-preserving federated learning. In *Proceedings of the IEEE/CVF international conference on computer vision*, pages 15076–15086, 2021.
- [59] Wenhui Wang, Furu Wei, Li Dong, Hangbo Bao, Nan Yang, and Ming Zhou. Minilm: Deep self-attention distillation for task-agnostic compression of pre-trained transformers. *Advances in neural information processing systems*, 33:5776–5788, 2020.
- [60] Sang Michael Xie and Stefano Ermon. Reparameterizable subset sampling via continuous relaxations. *arXiv preprint arXiv:1901.10517*, 2019.
- [61] Hugo Touvron, Matthieu Cord, and Hervé Jégou. Deit iii: Revenge of the vit. In *European conference on computer vision*, pages 516–533. Springer, 2022.

A Appendix

A.1 Adaptive Token Method Descriptions

A.1.1 Token Reduction

Protect Informative Tokens before Merging (PiToMe) [23] builds on Bipartite Soft Matching (BSM), which partitions tokens into two sets and merges pairs across both according to key-based similarity. Instead of considering *all* tokens for merging, PiToMe proposes an energy score—defined as an aggregate similarity of a token with all others—to distinguish redundant (high-energy) from informative (low-energy) tokens. Only the top $2k$ high-energy tokens are considered for merging via BSM, preserving the most informative tokens.

Agglomerative Token Clustering (ATC) [24] replaces BSM with a bottom-up, hierarchical clustering approach for token merging. Each token starts as its own cluster, and clusters are iteratively merged based on a similarity score defined between clusters. At each step, the two most similar (i.e., redundant) clusters are merged, continuing until a target number of tokens remains.

Decoupled Token Embedding for Merging (DTEM) [25] introduces a trainable module that decouples token merging from representation learning. It projects intermediate token embeddings to extract merging-specific features for estimating pairwise token similarities. Unlike traditional *hard* assignment grouping schemes, DTEM uses a differentiable top- k operator [60] to softly group tokens, followed by BSM for merging. Notably, the soft merging retains *all* tokens during training, with discretization applied only during inference for actual token reduction.

A.1.2 Patch Selection

PatchDrop [27] formulates selection as a Reinforcement Learning problem to train a patch selection policy. Given a down-sampled input, the policy returns Bernoulli distributions over high-resolution patches from which samples are drawn. The policy is initially trained using the REINFORCE [50] algorithm with a *fixed* pretrained classifier, receiving rewards that encourage both classification accuracy and sparse sampling. A joint finetuning stage then updates the policy and classifier together for improved performance.

Differentiable Patch Selection (DPS) [28] casts patch selection as a ranking problem, where a scoring network assigns relevance scores to high-resolution patches based on a low-resolution input. A differentiable top- k module, based on the perturbed maximum method [54], selects the top k scoring patches for downstream processing by feature and patch-aggregation networks. The entire pipeline is trained end-to-end under supervision.

Iterative Patch Selection (IPS) [29] performs ranking-based patch selection directly on the high-res input through sequential glimpses. A scoring module maintains a buffer of the top k most salient patches, which is updated auto-regressively by evaluating I patches at a time in no-gradient mode. The selected patches are then re-embedded with gradients enabled and passed to a cross-attention transformer-based classifier, enabling end-to-end training. This same cross-attention module is shared with the scoring network to guide saliency prediction.

Learning to Rank Patches (LTRP) [30] trains a patch ranking model via self-supervision. Using a pretrained masked autoencoder, the method randomly masks patches and estimates each *visible* patch’s importance by measuring the change in image reconstruction when the patch is removed—yielding a pseudo-relevance score. A ranking model is then trained to predict the resulting ranks such that, following pretraining, they may be used to retain the top most salient patches for downstream tasks.

A.2 Experimental Details

A.2.1 Pretraining Hyperparameters

We pretrain our ViT-S for 400 epochs and ViT-B for 200 epochs on ImageNet-1K [31] using the AdamW optimizer [46]. We use a batch size of 1024, image size of 518×518 px, weight decay of 0.05, learning rate warmup of 10%, peak learning rate of $2e-04$ with cosine decay to $1e-05$, and RandAugment [47] data augmentation.

A.2.2 ImageNet Hyperparameters

We finetune for 30 epochs on ImageNet-1K [31] using the AdamW optimizer [46]. We use a batch size of 128, image size of 224×224 px, weight decay of 0.02, learning rate warmup of 10%, peak learning rate of $2e-5$ with cosine decay to $1e-5$, and 3-Augment [61] data augmentation.

A.2.3 ADE20K Hyperparameters

We finetune for 160K steps on ADE20K [32] using the AdamW optimizer [46]. We use a batch size of 16, image size of 518×518 px, weight decay of 0.02, learning rate warmup of 10%, peak learning rate of $2e-5$ with cosine decay to $1e-5$, and data augmentation: random crop scale $[0.7, 1.0]$, horizontal flip, random choice {gray scale, solarize, gaussian blur}, and color jitter (0.3). We compute all patch-token representations by interpolating sparse representations with the same interpolation method used during pretraining. We use a simple linear head that maps patch-token representations to pixel-wise class predictions.

A.2.4 Traffic Signs Recognition

Traffic Signs Setup. We use the annotated subset of the Swedish Traffic Signs dataset [33], containing 747 training and 684 test images. All images are resized and cropped to square dimensions of 994×994 px for compatibility with DINOv2 ViT backbones pretrained on square images. IPS and DPS use 980×980 px due to compatibility with their ViT patch extraction methods. We finetune all models for 30 epochs using the AdamW optimizer [46]. We sweep learning rates over $\{2e-5, 5e-5, 8e-5, 1e-4\}$ with a batch size of 16, following [29], and report the best final test accuracy achieved by each method. We apply a weight decay of 0.02, a 10% learning rate warmup, with cosine decay to $1e-05$, and data augmentation including random cropping (scale range $[0.8, 1.0]$) and standard RandAugment transformations [47]. DTEM and PiToMe merge tokens after every layer, ATC merges after layers 4, 7, and 10 (following [52]).

Traffic Signs Results in Tabular Format. We report the full experimental results in Table 3 to complement Figure 4.

Table 3: **Traffic Signs results.** LookWhere remains competitive with SoTA token selection methods, being more efficient than IPS and rivaling DPS for speed, memory, and FLOPs. LookWhere-R uses random masking instead of the selector, but still receives the selector’s low-res global tokens for context. DTEM runs out of memory (OOM).

Method	Top-1 Acc. % \uparrow	Memory (GB) \downarrow		FLOPs (G) \downarrow		Speed (im/s) \uparrow	
		Test	Train	Test	Train	Test	Train
DINOv2 [1]	94.0	3.1	21.3	900	2698	24.1	6.8
PiToMe [23] ($r=0.9$)	66.5	3.1	8.6	440	1300	51.4	17.0
ATC [24] ($r=0.7$)	69.3	2.7	10.7	537	1599	1.3	1.2
DTEM [25]	OOM	OOM	OOM	OOM	OOM	OOM	OOM
DPS ($r=0.1$) [28]	83.6	0.8	1.8	49	142	942.4	259.0
IPS ($r=0.1$) [29]	96.3	0.8	1.8	1819	1912	94.1	79.3
LookWhere-R ($k=504$)	70.6	0.8	1.8	53	149	609.8	222.0
LookWhere ($k=504$)	94.6	0.8	1.8	53	149	609.8	222.0
LookWhere ($k=1008$)	95.2	0.9	2.5	110	320	288.1	99.1

A.2.5 Fine-grained Bird Classification

Fine-grained Bird Classification Setup. We finetune for 30 epochs on the Caltech-UCSD Birds (CUB-200-2011) dataset [40] of 200 bird species in 11,788 images. We sweep learning rates over $\{2e-5, 5e-5, 8e-5, 1e-4\}$ using a batch size of 64. Images are resized to 518×518 px by default (588×588 px for IPS and DPS for 98×98 pixel patches fed to the ViT feature extractor). We use a weight decay of 0.02, a 10% learning rate warmup, and cosine decay to a minimum learning rate of $1e-05$. Data augmentation includes random cropping (scale range $[0.8, 1.0]$) and standard RandAugment transformations [47]. DTEM and PiToMe merge tokens after every layer, ATC merges after layers 4, 7, and 10 (following [52]).

Detailed Bird Results in Tabular Format. We report the full experimental results in Table 4 to complement Figure 4.

Table 4: **Bird results.** LookWhere achieves the Pareto frontier with the fastest speed, and lowest memory and FLOPs among SoTA token reduction and selection methods while retaining competitive accuracy. LookWhere-R uses random masking instead of the selector, but still receives the selector’s low-res global tokens for context.

Method	Top-1 Acc.	Memory (GB) ↓		FLOPs (G) ↓		Speed (im/s) ↑	
	% ↑	Eval	Train	Eval	Train	Eval	Train
DINOv2 [1]	90.5	0.9	3.1	152	455	209.4	67.4
PiToMe [23] ($r=0.9$)	34.3	0.9	1.9	81	239	391.1	128.4
ATC [24] ($r=0.7$)	34.4	0.9	2.1	95	285	21.2	18.2
DTEM [25] ($r=96$)	90.7	1.0	5.5	84	464	261.8	52.3
DPS ($r=0.1$) [28]	85.4	0.7	1.8	19	57	2479.0	697.7
DPS ($r=0.2$)	88.3	0.7	1.8	33	98	1442.2	432.1
IPS ($r=0.1$) [29]	89.0	0.8	1.8	653	690	261.8	213.8
IPS ($r=0.2$)	90.2	0.8	1.8	639	704	241.8	179.4
LookWhere-R ($k=136$)	78.2	0.8	1.7	16	41	2322.4	865.6
LookWhere ($k=136$)	89.0	0.8	1.7	16	41	2322.4	865.6
LookWhere ($k=273$)	89.8	0.8	1.7	29	19	1333.6	479.0

A.3 Detailed Ablation Setup and Results

We ablate several design choices, including: (1) teacher attention targets for selector maps, (2) distillation loss weights, (3) selector map training schemes, (4) low-resolution conditioning tokens for the extractor, and (5) the input size and depth of the selector. Unless stated otherwise, all ablations are conducted over 400 epochs of pretraining on ImageNet-1K [31] at a resolution of 518×518 pixels using the ViT-S architecture. During pretraining, we sample $k \in [16, 128]$ uniformly at random, and report results at test time for fixed values $k \in \{16, 72, 128\}$ for general classification and segmentation downstream tasks. Unless stated otherwise, ablations use our default settings, which are highlighted in blue.

To ablate LookWhere efficiently, we use a simple k NN-based evaluation. For classification, we process all ImageNet-HR [48] images with LookWhere and store the resulting class-token representations $\hat{z}_{\text{high}}^{\text{cls}}$. We then compute top-1 accuracy using a leave-one-out k NN approach; specifically, for each ImageNet-HR image, we retrieve the 3 nearest neighbors, excluding the query itself and assign the most frequent class among them as the prediction. For segmentation, we process all ADE20K [32] images with LookWhere and store 10 patch-token representations $\hat{z}_{\text{high}}^{\text{pat}}$ per sample. We then compute top-1 accuracy using the validation set as queries and the training set as keys. We fetch 20 patch tokens for each query and assign the most common class as the predicted label.

A.3.1 Teacher Attention Targets for Selection

To distill the teacher’s attention, we extract the unnormalized attention among its patch tokens at *select* layers and query tokens and then average over layers, queries and heads (Fig. 8). This approximates where the selected patches contributed to the teacher representation. In this section, we explore different combinations of *layers* and *query tokens* used for attention aggregation.

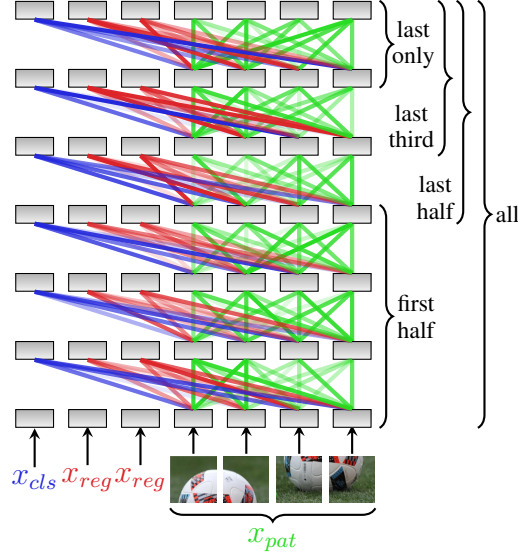


Figure 8: **Attention Aggregation.** We aggregate attention by averaging unnormalized attention scores originating from the **cls**, **reg**, and **patch** queries across different layers (all, first 3, last 3, last 2, and last only). Score maps from each query type are weighted equally when several are used (i.e., we average the maps among tokens of each type first, before averaging across types).

Classification		Layer Aggregation				
Query Aggregation		first half	last half	last third	last only	all layers
	cls	48.5	52.9	54.8	57.6	52.1
	reg	47.8	50.1	50.8	56.5	49.2
	pat	46.9	49.8	50.3	54.1	48.8
	cls+reg	48.5	49.0	53.8	57.2	50.9
	cls+pat	48.9	52.2	54.2	57.7	50.8
	reg+pat	47.5	49.4	51.0	56.3	48.6
	cls+reg+pat	47.9	51.5	52.8	57.3	51.3

Segmentation		Layer Aggregation				
Query Aggregation		first half	last half	last third	last only	all layers
	cls	52.3	51.8	51.6	51.8	52.1
	reg	53.4	53.2	52.7	52.2	53.7
	pat	53.6	54.2	53.6	53.3	54.1
	cls+reg	53.4	52.2	52.5	51.7	53.0
	cls+pat	52.5	52.7	52.6	52.3	52.7
	reg+pat	53.6	53.1	53.6	53.2	53.9
	cls+reg+pat	53.8	53.1	52.1	52.0	53.4

Figure 9: **Teacher Attention for Selection** ($k=16$). We evaluate teacher attention maps as selector maps to choose distillation targets when testing using $k=16$ selected patches.

		Layer Aggregation				
		first half	last half	last third	last only	all layers
Query Aggregation	cls	65.0	68.6	69.2	70.3	67.8
	reg	64.1	66.2	66.8	70.2	65.5
	pat	62.4	69.0	68.9	70.4	67.5
	cls+reg	65.4	66.4	68.8	70.4	67.1
	cls+pat	65.0	68.9	69.6	70.9	68.3
	reg+pat	64.1	67.5	68.4	70.6	66.6
	cls+reg+pat	64.9	68.0	69.2	70.6	67.6

		Layer Aggregation				
		first half	last half	last third	last only	all layers
Query Aggregation	cls	61.4	60.8	60.4	59.4	60.8
	reg	61.1	61.5	61.6	60.5	62.1
	pat	62.1	64.2	63.7	62.7	64.2
	cls+reg	61.2	61.0	61.0	60.1	62.2
	cls+pat	62.0	62.0	61.0	60.9	62.0
	reg+pat	61.7	62.4	62.7	61.1	62.6
	cls+reg+pat	61.5	62.2	61.4	60.5	62.4

Figure 10: **Teacher Attention for Selection** ($k=72$). We evaluate teacher attention maps as selector maps to choose distillation targets when testing using $k=72$ selected patches.

		Layer Aggregation				
		first half	last half	last third	last only	all layers
Query Aggregation	cls	69.3	72.1	72.4	73.4	71.9
	reg	69.1	70.2	71.3	73.4	69.6
	pat	67.0	71.9	72.0	73.1	71.6
	cls+reg	69.3	70.4	72.7	73.7	71.2
	cls+pat	69.6	72.6	73.0	73.7	72.0
	reg+pat	68.9	71.3	72.1	74.3	70.9
	cls+reg+pat	69.2	72.2	73.0	73.4	71.6

		Layer Aggregation				
		first half	last half	last third	last only	all layers
Query Aggregation	cls	64.3	63.8	63.4	63.4	64.5
	reg	64.5	64.9	65.0	64.1	65.2
	pat	65.5	67.4	67.3	66.2	67.5
	cls+reg	64.5	64.7	64.8	63.2	65.2
	cls+pat	65.4	65.7	64.9	63.7	65.7
	reg+pat	65.1	66.0	66.1	64.6	66.1
	cls+reg+pat	64.9	65.8	65.2	63.8	65.8

Figure 11: **Teacher Attention for Selection** ($k=128$). We evaluate teacher attention maps as selector maps to choose distillation targets when testing using $k=128$ selected patches.

A.3.2 Classification Accuracy vs. Distillation Losses

We ablate distillation weights and feature-interpolation parameters with 100 epochs of pretraining. During pretraining (and when using ADE20K downstream), we interpolate the sparse/visible high-res patch-token representations to compute a full 2D grid. We compute the predicted dense patch-token representations as the weighted sum of the N nearest neighbors in 2D space, among the sparse/visible patch tokens. The weights in the weighted sum are the Euclidean distances raised to the pow^{th} power, then normalized s.t. all weights sum to 1. We experiment with $N \in \{5, 16\}$ and $\text{pow} \in \{1, 2\}$, and summarize our results in Tables 5 through 8.

Table 5: **Distillation Losses** ($\text{pow}=1, 5$ neighbors). We evaluate different combinations of distillation loss weights for pretraining the selector-extractor ($\lambda_{cls}, \lambda_{pat}$) and selector map (λ_{map}). We consider spatial patch interpolation using Euclidean distance, with 5 selected neighbours.

λ_{cls}	λ_{pat}	λ_{map}	\mathcal{L}_{map}	cls. (by k)			seg. (by k)		
				16	72	128	16	72	128
1	1	1	KL	47.7	61.7	66.4	51.6	59.6	62.6
1	1	0.1	KL	46.8	61.5	66.7	51.0	59.5	62.3
1	0.1	1	KL	48.1	62.5	67.4	48.2	57.3	60.8
1	0.1	0.1	KL	48.9	63.0	67.4	47.8	56.7	60.7
0.1	1	1	KL	44.9	60.3	66.1	51.6	59.8	63.4
0.1	1	0.1	KL	45.0	60.2	65.3	51.3	59.7	62.9
0.1	0.1	1	KL	46.1	62.2	66.9	51.0	59.5	63.1
0.1	0.1	0.1	KL	48.7	62.0	66.7	50.8	59.8	62.5
1	1	1	MSE	50.2	61.8	66.2	51.2	58.5	62.0

Table 6: **Distillation Losses** ($\text{pow}=1, 16$ neighbors). We evaluate different combinations of distillation loss weights for pretraining the selector-extractor ($\lambda_{cls}, \lambda_{pat}$) and selector map (λ_{map}). We consider spatial patch interpolation using Euclidean distance, with 16 selected neighbours.

λ_{cls}	λ_{pat}	λ_{map}	\mathcal{L}_{map}	cls. (by k)			seg. (by k)		
				16	72	128	16	72	128
1	1	1	KL	48.9	62.2	66.8	49.4	58.1	61.5
1	1	0.1	KL	48.1	61.9	66.9	48.9	57.4	61.0
1	0.1	1	KL	47.4	62.4	67.0	47.4	56.7	60.2
1	0.1	0.1	KL	48.3	62.2	66.2	47.5	55.9	60.2
0.1	1	1	KL	44.6	60.4	65.5	49.8	58.8	62.0
0.1	1	0.1	KL	45.8	60.0	66.0	49.2	58.5	61.6
0.1	0.1	1	KL	46.5	62.6	67.0	49.0	58.2	62.1
0.1	0.1	0.1	KL	47.8	62.5	67.1	49.6	58.4	61.6

Table 7: **Distillation Losses** ($\text{pow}=2, 5$ neighbors). We evaluate different combinations of distillation loss weights for pretraining the selector-extractor ($\lambda_{cls}, \lambda_{pat}$) and selector map (λ_{map}). We consider spatial patch interpolation using squared Euclidean distance, with 5 selected neighbours.

λ_{cls}	λ_{pat}	λ_{map}	\mathcal{L}_{map}	cls. (by k)			seg. (by k)		
				16	72	128	16	72	128
1	1	1	KL	46.7	61.9	67.2	50.7	59.0	62.8
1	1	0.1	KL	47.0	61.5	65.8	50.5	59.6	62.5
1	0.1	1	KL	49.3	62.6	67.0	48.3	56.7	60.6
1	0.1	0.1	KL	48.0	62.6	67.2	48.3	56.7	60.6
0.1	1	1	KL	44.8	60.6	66.0	48.0	56.5	48.0
0.1	1	0.1	KL	43.9	60.3	65.1	51.3	59.8	63.2
0.1	0.1	1	KL	45.7	62.3	67.0	50.6	59.0	62.5
0.1	0.1	0.1	KL	47.6	62.3	66.3	50.7	59.1	62.6

Table 8: **Distillation Losses** (pow=2, 16 neighbors). We evaluate different combinations of distillation loss weights for pretraining the selector-extractor (λ_{cls} , λ_{pat}) and selector map (λ_{map}). We consider spatial patch interpolation using squared Euclidean distance, with 16 selected neighbours.

λ_{cls}	λ_{pat}	λ_{map}	\mathcal{L}_{map}	cls. (by k)			seg. (by k)		
				16	72	128	16	72	128
1	1	1	KL	48.3	62.1	66.9	50.2	58.2	61.7
1	1	0.1	KL	47.6	61.5	66.4	49.8	57.5	61.6
1	0.1	1	KL	48.7	62.6	67.5	47.7	56.7	60.1
1	0.1	0.1	KL	49.1	62.6	66.9	47.6	6.1	59.8
0.1	1	1	KL	44.1	61.0	65.3	50.4	59.5	62.6
0.1	1	0.1	KL	44.2	60.8	65.7	50.4	58.8	61.7
0.1	0.1	1	KL	45.9	62.3	67.2	49.8	58.4	62.2
0.1	0.1	0.1	KL	47.8	62.5	67.1	50.3	58.7	62.2

A.3.3 Selector Map Training

In addition to distilling the teacher’s attention map, we explore differentiable learning of the selector map to better leverage the extractor’s signal for optimal patch selection. To enable differentiable selection, we experiment with (1) Gumbel Top-K [49] and (2) REINFORCE [50].

In both approaches, the selector map is treated as logits defining a softmax probability distribution over patches; we sample the map using the Gumbel Top-K trick. We make sampling differentiable through the straight-through estimator (i.e., differentiable Gumbel Top-K) and sweep over learning rates and sampling temperatures. With REINFORCE, we model pretraining as a one-step (contextual) bandit problem: low-resolution images define the state, actions are binary masks selecting k patches (as in PatchDrop [27]), and the reward is derived from the loss. Specifically, we compute an advantage as the difference in distillation loss between a greedy top- k policy and the sampled action. We backpropagate through the extractor for both samples. We explore various learning rates, weightings for distillation and policy gradient losses, and the use of an entropy bonus to promote exploration.

We observe that training fails to converge without a map distillation loss (which effectively acts analogous to a KL regularizing term with respect to the teacher’s “policy”). Table 9 reports the best results across all configurations, consistently showing that teacher distillation alone performs best. Gumbel Top-K pretrains for 400 epochs, while REINFORCE pretrains for 300 epochs (to roughly balance compute across all methods since REINFORCE backpropagates through both the policy sample and greedy baseline).

Table 9: **Selector Map Training Schemes**. We consider different training schemes for the selector map *in addition to distillation*. Stop grad refers to no additional scheme, while Gumbel Top-K and REINFORCE leverage sampling to estimate a gradient from the extractor’s signal. We find that distillation, alone, is optimal.

case	cls. (by k)			seg. (by k)		
	16	72	128	16	72	128
none (stop grad)	50.9	63.0	66.5	51.1	60.2	62.9
Gumbel Top-K [49]	44.5	61.4	66.2	49.1	58.9	62.5
REINFORCE [50]	47.9	61.8	66.0	50.7	59.6	62.8

A.3.4 Extractor Conditioning on Low-Resolution Global Tokens

To provide the extractor with additional *global* image context, we experiment with initializing its class token x_{cls} and/or register tokens x_{reg} by the selector’s final representations for each: z_{low}^{cls} and z_{low}^{reg} , respectively. Table 10 summarizes our results; we find that adding global tokens generally helps, although performance interestingly degrades for classification when selecting $k=128$ patches specifically.

Table 10: **Extractor Conditioning.** We experiment with feeding the extractor different combinations of global low-resolution tokens resulting from the selector’s processing. We find that giving *both* the cls token and all register generally helps performance.

case	cls. (by k)			seg. (by k)		
	16	72	128	16	72	128
none	28.2	60.7	68.4	39.7	56.9	61.1
cls-only	48.8	62.2	67.2	49.8	58.7	61.8
reg-only	49.4	62.0	67.3	51.0	59.8	62.4
cls+reg	50.9	63.0	66.5	51.1	60.2	62.9

A.3.5 Extractor Input Size and Depth

We experiment with varying the extractor’s size by trading off network depth against input resolution while keeping computational cost relatively low. Our results are summarized in Table 11.

Table 11: **Extractor Sizes.** Both shallow networks with large inputs and deeper networks with smaller inputs result in suboptimal performance. The best results are achieved by balancing depth and input resolution.

depth	res.	cls. (by k)			seg. (by k)		
		16	72	128	16	72	128
1	252^2	43.7	66.2	70.8	49.0	60.5	64.4
3	252^2	65.8	72.1	73.7	56.1	64.7	67.2
3	154^2	58.7	68.8	71.2	53.9	62.7	65.1
6	154^2	65.0	69.7	72.1	54.4	63.0	65.4
6	98^2	50.9	63.0	66.5	51.1	60.2	62.9
12	98^2	65.8	69.6	70.9	53.0	61.0	63.3
12	42^2	25.5	47.3	57.1	43.8	54.6	58.1

A.4 Selector Maps

Our selector generalizes to diverse downstream images and tasks. In particular, we visualize general examples for the recognition of birds (Fig. 12) and traffic signs (Fig. 13).

A.4.1 Bird Recognition (CUB) Selector Maps

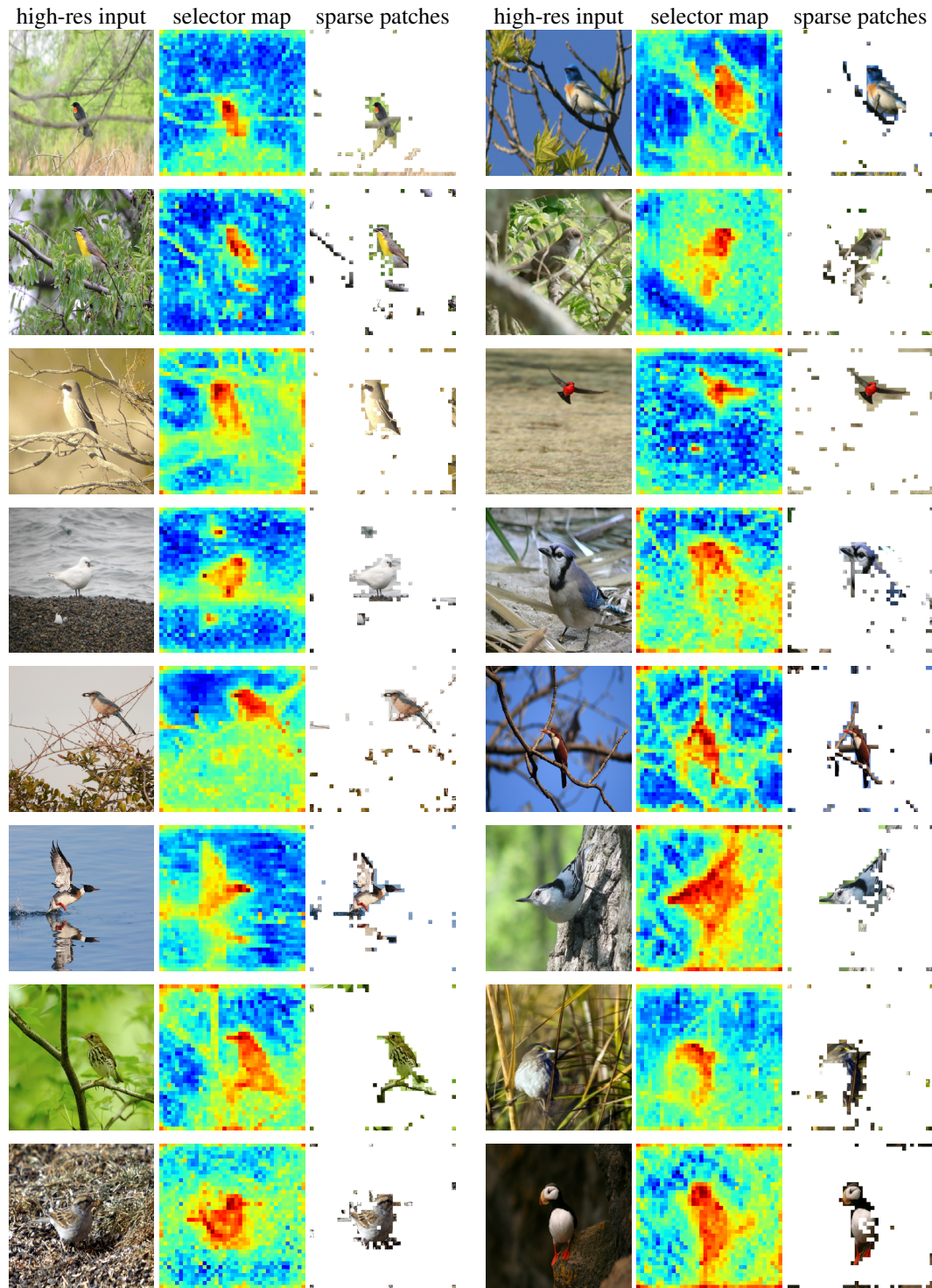


Figure 12: **Adaptive Computation for Recognizing Birds.** We visualize the selector’s prediction of *where* to compute and the extractor’s sparse input for *what* to see. We do *not* finetune the selector; each pair shows different generalization scenarios, specifically for bird recognition on CUB [40].

A.4.2 Traffic Signs Selector Maps

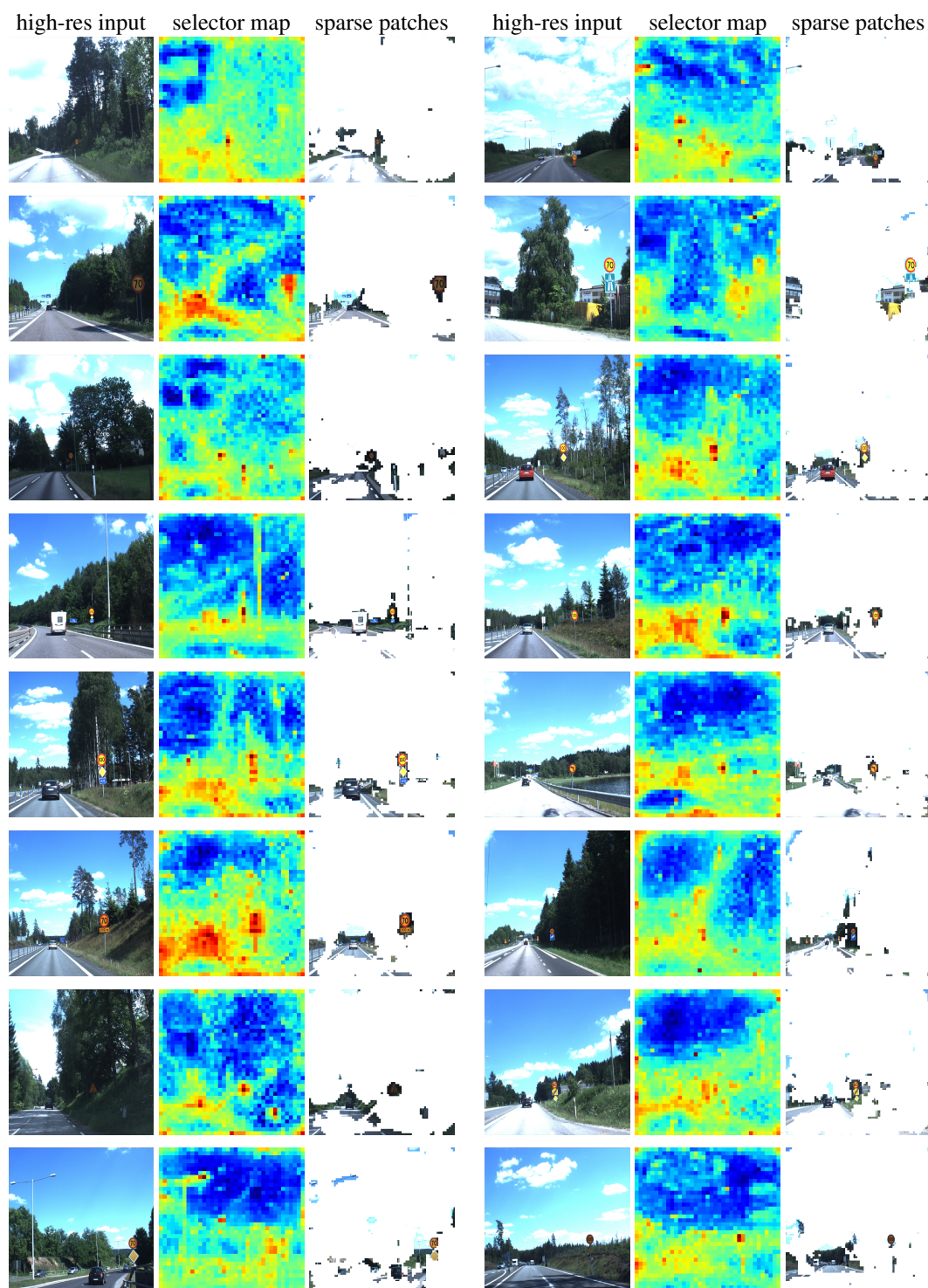


Figure 13: **Adaptive Computation for Traffic Sign Recognition.** We visualize the selector’s prediction of *where* to compute and the extractor’s sparse input for *what* to see. We do *not* finetune the selector; each pair shows different generalization scenarios, specifically for recognizing traffic signs on the Swedish Traffic Signs dataset [33].